Continuous wave cavity ring down spectroscopy measurements of velocity distribution functions of argon ions in a helicon plasma

Saikat Chakraborty Thakur, Dustin McCarren, Jerry Carr, Jr., and Earl E. Scime
Department of Physics, West Virginia University, Morgantown, West Virginia 26506, USA

(Received 13 September 2011; accepted 2 February 2012; published online 27 February 2012)

We report continuous wave cavity ring down spectroscopy (CW-CRDS) measurements of ion velocity distribution functions (VDFs) in low pressure argon helicon plasma (magnetic field strength of 600 G, $T_e \approx 4$ eV and $n \approx 5 \times 10^{11}$ cm^{-3}). Laser induced fluorescence (LIF) is routinely used to measure VDFs of argon ions, argon neutrals, helium neutrals, and xenon ions in helicon sources. Here, we describe a CW-CRDS diagnostic based on a narrow line width, tunable diode laser as an alternative technique to measure VDFs in similar regimes but where LIF is inapplicable. Being an ultra-sensitive, cavity enhanced absorption spectroscopic technique; CW-CRDS can also provide a direct quantitative measurement of the absolute metastable state density. The proof of principle CW-CRDS measurements presented here are of the Doppler broadened absorption spectrum of Ar II at 668.6138 nm. Extrapolating from these initial measurements, it is expected that this diagnostic is suitable for neutrals and ions in plasmas ranging in density from 1×10^9 cm^{-3} to 1×10^{13} cm^{-3} and target species temperatures less than 20 eV. © *2012 American Institute of Physics*. [http://dx.doi.org/10.1063/1.3687429]

INTRODUCTION

The relatively high plasma densities ($>10^{13}$ cm^{-3}) and the possibility to either supply an independent voltage to a sample substrate or to allow a sample holder to electrically float are characteristics that make helicon sources particularly attractive as plasma processing sources. For material processing applications involving deposition, surface modification or etching, control of the ion temperature, ion speed, plasma density, and uniformity in the expanding plasma (downstream of the plasma source) are of utmost importance. In processing applications, helicon plasma sources have been shown to generate uniform plasma fluxes with reduced ion energies at a substrate in a downstream diffusion chamber.[1–3] Arrays of compact helicon plasma sources can produce uniform plasmas over even larger surface areas.[4] For plasma etching, high etching rates (1.5 μm/min) with minimal anisotropy (0.97) were obtained with an expanding SF_6 helicon plasma.[5] However, improved control of ion flow speed and ion temperature and an improved understanding of charge exchange collisions in the expansion region are needed for helicon sources to become competitive with more technologically mature, commercially available plasma processing systems.

The CHEWIE (compact helicon waves and instabilities experiment) experiment is specifically designed to explore the properties of helicon sources in a plasma processing relevant geometry and as a test bed for developing new velocity distribution function (VDF) diagnostics for ions and neutrals. Key parameters such as relative density, temperature, flow velocity, and the relative density of any energetic tails in the velocity distribution are calculable from measurements of the VDF of neutral or ion species in the plasma.

There are multiple, *in situ*, experimental techniques for measuring VDFs or energy distribution functions (EDFs); each with its own advantages and disadvantages. The retarding field energy analyzer (RFEA) is a standard *in situ* probe technique used to measure ion and electron EDFs along the background magnetic field in low density, low temperature plasmas.[6] Even though RFEAs are perturbative, they are simple to construct and relatively easy to use. Since a RFEA probe can quickly overheat in a dense laboratory plasma, RFEAs are typically employed in low density plasmas or at the edges of higher density, short pulse plasma devices. A RFEA is incapable of measuring the EDF of neutrals and cannot distinguish between ions of different species. RFEA measurements of ion and electron EDFs perpendicular to the background magnetic field are also problematic because the particle gyroradius is a function of the particle velocity. Therefore regions of energy space are blocked from entering the RFEA aperture by the probe head itself. In a previous work, we compared ion EDF measurements obtained with a RFEA and ion VDF measurements obtained with laser induced fluorescence (LIF) in argon plasmas.[7] Those experiments demonstrated that while the RFEA more easily detected the presence of energetic ion beams in the plasma, the RFEA measurements of parallel ion temperature were heavily distorted by fluctuations in the sheath potential that formed between the front plate of the RFEA and the plasma.

The classic Langmuir probe is essentially a RFEA device for both electrons and ions. Charged particles with sufficient energy to overcome the potential applied to the Langmuir probe are collected and the current measured. Although it is possible to extract some details about the electron EDF from a Langmuir probe current versus voltage sweep,[8] the details of the ion EDF are much harder to extract from Langmuir probe measurements; neutral EDFs cannot be measured with a Langmuir probe; and any flows in the plasma make the interpretation of the electron EDF particularly problematic.[9]

LIF is routinely employed in helicon[10–12] and other plasma sources to measure velocity distributions of argon ions, argon neutrals, helium neutrals, and xenon ions.[13–15]

LIF is an effective and versatile technique as long as sufficiently large populations of the target species initial state are available. Hence, the target initial state is typically a metastable state. Yet for many ion and neutral species and at low temperatures and densities, the signal-to-noise ratio of the available LIF scheme is insufficient for a reliable VDF measurement. To address this limitation, we have developed a continuous wave cavity ring down spectroscopy (CW-CRDS) diagnostic based on a narrow line width, tunable diode laser. CW-CRDS provides the sensitivity needed to measure VDFs for species inaccessible by conventional LIF at the expense of a loss of spatial localization (in one dimension) of the measurement.

Over the last two decades, cavity ring down spectroscopy (CRDS) (Ref. 16) has widely been used as a highly sensitive absorption technique for measuring very low concentrations of specific gasses. CRDS is a resonant cavity enhanced absorption measurement technique in which the analyte to be detected is placed inside the resonant cavity and the absorption of light by the sample detected. The interested reader is referred to some excellent reviews on the progress of CRDS.[17–21] Perhaps the most relevant applications of CRDS to the work presented here are elemental and isotopic measurements using CRDS combined with a plasma source to create the gaseous sample.[22] With the replacement of cumbersome pulsed dye lasers with smaller, less expensive, continuous wave (CW) diode lasers, CW-CRDS systems have become more widely used as analytical tools.[23] CW-CRDS is experimentally more challenging than conventional CRDS using pulsed lasers, but the increased flexibility and lower cost of CW-CRDS systems more than compensate for the added measurement complexity. CW-CRDS has been used as a diagnostic tool for atmospheric plasma discharges,[22] elemental detection[24] and broadband molecular spectroscopy.[21] The few implementations of CW-CRDS in plasmas in high vacuum environments have typically focused on target species detection and not wavelength resolved velocity distribution measurements of the plasma characteristics. CW-CRDS velocity distribution function measurements in a plasma require a narrow linewidth, tunable, CW laser; a high finesse optical cavity surrounding the plasma column; and a means of moving the cavity defining mirrors inside the vacuum environment. Although CW-CRDS has been implemented in a few plasma sources, there do not appear to be published reports of measurements of argon plasma velocity distributions in any plasma device or for any gas in a helicon source. In this paper, we describe the details of our CW-CRDS apparatus and report the first CW-CRDS measurements of argon ion VDFs through Doppler resolved spectroscopy of argon ions in low pressure helicon plasma.

EXPERIMENTAL APPARATUS

The CHEWIE plasma source consists of a vertically oriented Pyrex glass tube 61 cm long and 7.5 cm in diameter coaxially mated to a stainless steel expansion chamber; 30 cm in length and 15 cm in diameter (Fig. 1). Three water cooled electromagnets produce a steady state axial magnetic field of 0–1000 G in the source. Rf power of up to 1.5 kW over a frequency range of 6–18 MHz is coupled into a 12.5 cm long $m = +1$ half-wave right-handed helical antenna wrapped around the outside of the Pyrex vacuum chamber, starting at ~22 cm from the top of the source chamber, to create the steady state plasma.

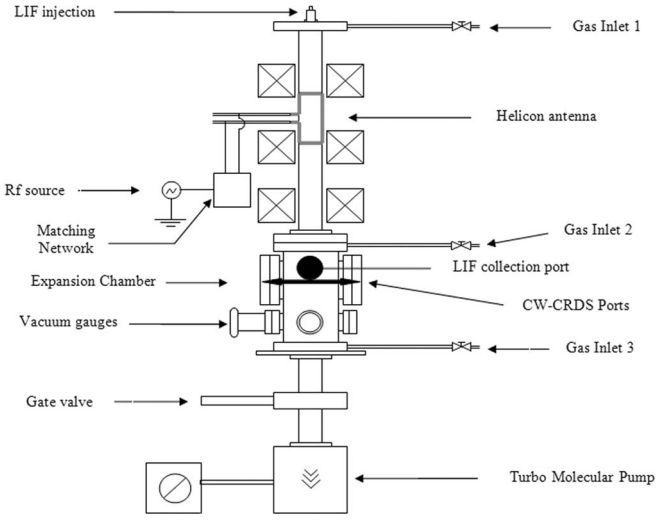

FIG. 1. Schematic of the helicon source CHEWIE. The thick black arrow identifies the path of the beam in the CW-CRDS cavity. The blackened port marks the location of the LIF measurements.

Vacuum is maintained with a turbo molecular pump at the bottom of the assembly, backed with an XtraDry 150-2 dry piston roughing pump. Typical base pressures achieved in the chamber are $\sim 10^{-7}$ Torr. The gas flow into the chamber is regulated with a MKS PR4000 power supply and a MKS 1179A mass flow controller. There are three locations where the gas can be fed into the device: at the top of the source chamber, at the junction between the source and expansion chambers, and at the bottom of the expansion chamber (as shown in Fig. 1). The smallest sustainable gas injection rate into the chamber is 11 SCCM (standard cubic centimeters per minute). During operation, the gas pressure is monitored with either a thermocouple or an ion gauge depending on the working pressure in the chamber.

LIF injection optics are mounted on a window at the top of the glass chamber. The top of the chamber is defined as the $z = 0$ position in CHEWIE. The expansion chamber has several ports which are used for diagnostic access. A rf-compensated Langmuir probe and the LIF collection optics are mounted on two of the 2.75 in. ports on the upper portion of the expansion chamber. Just below those ports, ~6 cm, the mirror holders for the CW-CRDS system are mounted on two opposing 6 in. ports. Further down the chamber, additional ports are used for other diagnostics and the pressure gauges. Characteristic electron temperature and plasma densities in the expansion region of CHEWIE, as measured with a rf compensated,[25] cylindrical Langmuir probe, are $T_e \approx 4$ eV and $n \approx 5 \times 10^{11}$ cm^{-3}.

At the most fundamental level, a CRDS system consists of a resonant optical cavity that surrounds the material to be sampled and a coherent light source. If the laser light is mode matched and injected into the high-finesse optical cavity, the light intensity inside the cavity builds up over

time due to constructive interference.[17] The high-finesse optical cavity is created from two high reflectivity mirrors ($R > 99.9\%$) and the reflection of light back and forth between the mirrors gives an effective path length of thousands of meters through the sample. When the laser is turned off, the intensity of light leaking out from the high reflectivity mirrors decays exponentially. For a cavity of length L made from two mirrors of each with reflectivity R, the ring down time τ is defined as the time required for the exponentially decaying light intensity to fall to $1/e$ of the initial intensity,

$$\tau = \frac{L}{c\,(1 - R + \alpha d)}, \tag{1}$$

where α is the frequency dependant absorption coefficient of the medium in the cavity. It is assumed that the absorbing sample is present only over a length d in the cavity and that the sum of losses in the mirrors and plasma is less than unity, i.e., this technique would not be applicable to plasmas with an optical thickness at the target wavelength much shorter than the cavity length.

In a typical CRDS experiment, the cavity ring down time is measured as a function of the laser frequency. The maximum change in the ring down time, with respect to the case when there is no absorber in the cavity, occurs when the laser frequency is tuned to the peak of the absorption line. The absorption spectrum is obtained by plotting the cavity decay rate $k = 1/\tau$ (or the cavity loss $1/c\tau$) as a function of frequency,

$$\frac{1}{c\tau\,(\nu)} = \frac{(1 - R)}{L} + \alpha\,(\nu)\,\frac{d}{L}. \tag{2}$$

The cavity loss is the sum of two terms. The first is the mirror loss and this term sets the minimum loss in the CRDS instrument. The second term is the absorption by the sample. The first term is often rewritten as the "off resonance mirror loss" and it is the effective loss without the presence of any absorbers in the cavity

$$\tau_0 = \frac{L}{c\,(1 - R)} = \frac{1}{k_0}. \tag{3}$$

The absorption due to the sample in the cavity is then given by the difference between the off-resonance and the on-resonance decay time constants.

$$\alpha\,(\nu)\,\frac{d}{L} = \frac{k - k_0}{c} = \frac{1}{c}\left(\frac{1}{\tau} - \frac{1}{\tau_o}\right). \tag{4}$$

The cavity decay rate is measured with and without the sample to determine the absorption coefficient. The limiting sensitivity of a CRDS instrument is set by the minimum measurable difference in ring down times between the on and off resonance cases,

$$\left[\alpha\,(\nu)_{\min}\,\frac{d}{L}\right] = \frac{(k - k_0)_{\min}}{c} = \frac{\Delta k_{\min}}{c} = \frac{1}{c\tau_0^2}\Delta\tau_{\min} = \frac{1 - R}{L}\left(\frac{\Delta\tau_{\min}}{\tau_0}\right). \tag{5}$$

Therefore, the higher the mirror reflectivity and the longer the cavity, the more sensitive CRDS becomes for a fixed minimum decay time measurement resolution.

The CW-CRDS system is shown schematically in Fig. 2. The laser used is a Toptica TA 100 tunable diode laser consisting of a Littrow configuration master oscillator followed by a tapered amplifier. The laser has a line width of ~1 MHz and has a mode hop free tuning range of more than 30 GHz. The coarse tuning range spans nearly 5 nm. For these measurements, the laser was tuned to 668.6138 nm; corresponding to $3d^4\ F_{7/2}$ to $4p^4\ D_{5/2}$ level transition in Ar II. 60 dB optical isolators were inserted between the master oscillator and the amplifier and between the amplifier and the first optical component. A 10% sampling beamsplitter is used to sample the beam for continuous monitoring of the laser wavelength (not shown in Fig. 2) with a Bristol 621 wavemeter; at an accuracy of ±0.0001 nm. The wavemeter easily identifies mode hops during laser wavelength scanning and such scans are excluded

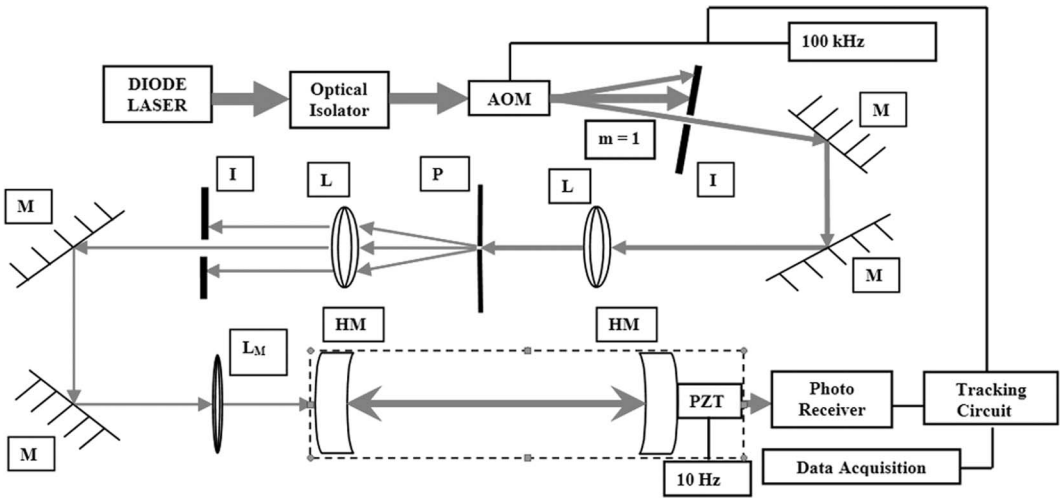

FIG. 2. Schematic of the CW-CRDS apparatus. I = iris, M = beam steering mirror, L = lenses used for spatial filtering, PH = pinhole, L_M = mode matching lens, HM = highly reflecting mirrors forming the optical cavity, AOM = acousto-optical modulator (100 kHz), PZT = Piezoelectric transducer (10 Hz). The mirrors and PZT are inside the vacuum chamber (indicated by dashed line).

from subsequent analysis. The primary beam is then injected into an acousto-optical modulator (AOM). The $m = 1$ mode of the AOM diffraction pattern is steered towards the CRDS cavity while an iris blocks the other diffraction modes. The highly elliptical laser light is shaped into a Gaussian beam with a spatial filter and the light is then injected into the optical cavity through a mode matching lens of focal length 75 cm (the focal point of the lens is placed at the midpoint of the cavity). The optical cavity is formed by two Los Gatos mirrors ($R = 99.97\%$) mounted on opposite sides of the CHEWIE expansion chamber. The mirrors are inside the vacuum chamber. The mirror holding flanges are connected to the chamber by welded bellows to permit mirror alignment while the system remains under vacuum. One of the mirrors was mounted on a linear piezoelectric transducer (PZT), driven at 10 Hz, for cavity length modulation. The total length of the optical cavity is 85 cm and the plasma fills the middle 20 cm of the cavity (the distance between the two ports in the 15 cm diameter expansion chamber). Several baffles were placed in front of the mirrors to reduce contamination of the mirrors by the plasma or the stainless steel deposits common to similar helicon devices. The light escaping through the far mirror passes through a 10 nm bandwidth filter and is focused onto the photodetector. The photodetector signal is recorded on a 16 bit digital oscilloscope.

At a given laser frequency, the cavity length is modulated (by scanning the mirror on the PZT) until one of the longitudinal modes of the cavity matches the laser wavelength and Gaussian intensity profile, i.e., the cavity length is an integer multiple of the laser wavelength. When a resonance occurs, the amplitude of the light in the cavity increases dramatically and the increase in the amplitude of the light escaping through the mirror triggers a custom tracking circuit that continuously monitors the photodetector signal. The tracking circuit (shown schematically in Fig. 3) controls the entire

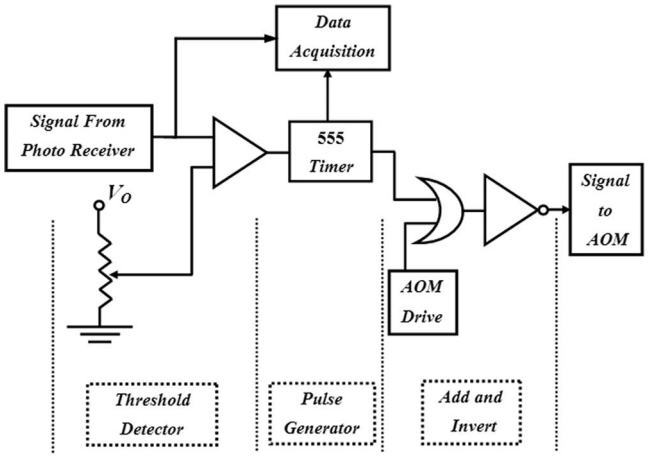

FIG. 3. Details of the tracking circuit: the first part is the threshold detector which compares the cavity output signal with respect to a standard voltage. The second part is a 555 timer which generates a TTL pulse as soon as the threshold detector is activated by a strong cavity output signal. This TTL pulse from the 555 timer triggers the data acquisition system and is added to the square wave AOM driving signal. The sum signal is inverted and sent to the AOM to force the AOM into the off state when the tracking circuit triggers. The comparator [LM 339N], 555 timer [NE555P], and the NOR gate [74HC02N] used are standard commercially available devices.

experimental sequence. Once the photodetector signal exceeds a user-specified threshold, a standard, commercially available, 555 pulse generator is triggered with the output of a voltage comparator. The pulse from the 555 is added, in the time domain, to the transistor-transistor logic (TTL) pulse sequence controlling the AOM. A NOT gate inverts the combined signal before sending the combined signal to the AOM driver. Thus, the addition of the 5 V pulse from the 555 forces the AOM drive signal to zero, effectively "turning off" the laser when the photodetector signal exceeds the predefined threshold. The width of the 555 pulse, typically set to ten times the expected ring down decay time, determines how long the laser light is turned off for the ring down decay measurement. At the end of the 555 pulse, the AOM control signal is restored, laser light again passes through the AOM, and the cycle repeats.

Ideally, as the PZT slowly scans the cavity length defining mirror, the laser would only couple into a single well-defined longitudinal mode. For each longitudinal mode, there can be several transverse modes excited in a general optical cavity. These transverse cavity modes are the $TEM_{m,n}$ modes corresponding to Laguerre-Gaussian waves in cylindrical cavities.[17,26] The lowest order transverse mode TEM_{00} ($m = 0$, $n = 0$) has a Gaussian cross sectional profile. All other higher order transverse modes ($TEM_{m,n}$) are spatially broken up into a sub array of beams and are also less intense. The Gaussian TEM_{00} mode is preferentially excited in our CW-CRDS experiment. This can be achieved by matching the beam spot sizes in the cavity and the wave front radii of curvature of the laser radiation with the lowest order mode of the cavity. Experimentally, this is achieved by placing mode matching lenses before the cavity so that the beam entering the cavity mimics the radiation field of the mode supported by the cavity. A converging lens is used such that the collimated beam is focused at the center of the cavity (for symmetric mirrors with the same radius of curvature). However, vibrations from the vacuum pump and acoustical noise in the laboratory also bring high-order transverse modes into resonance with the injected laser light. The high-order transverse modes yield much smaller resonance peaks. By setting a high threshold for the tracking circuit, only coupling into the most resonant, purely longitudinal modes trigger a ring down measurement and the transverse modes are excluded from analysis. Each ring down measurement is an average of one hundred individual ring down decays. A typical measurement is shown in Fig. 4. The averaged decay curve is then fit with an exponential function to extract the time constant of the decay. For each laser wavelength, the ring down measurement is repeated ten times and the ten measurements averaged together.

The argon ion VDF is obtained by very slowly scanning the laser frequency through the absorption line. As the wavelength changes, the PZT (scanning back and forth at 10 Hz) allows the cavity to mode match to the injected laser light and the averaged ring down measurements are obtained for each wavelength step. Ring down time measurements with and without plasma are performed at each wavelength to isolate the contribution of the target plasma species to the measured absorption. As long as opposing ports are available, the

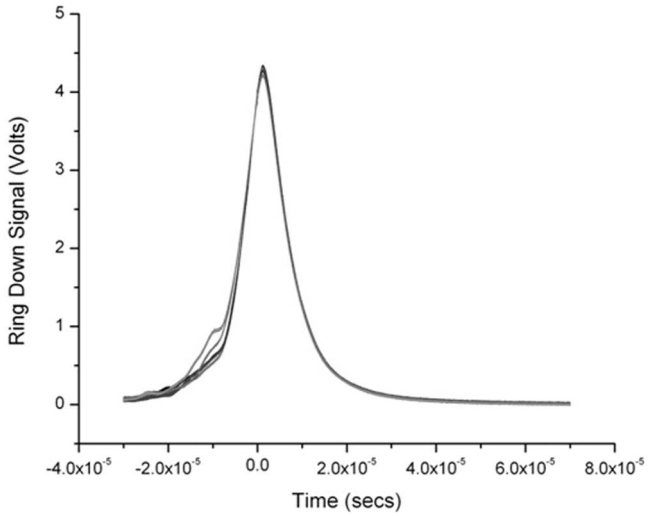

FIG. 4. Typical ring down measurement ($t > 0$) obtained at a single wavelength from the CW-CRDS system. The tracking circuit triggers and turns the laser injection off at $t = 0$. The four colors (online) show the consistency of cavity ring down signals obtained at different times but at the same wavelength. Each curve is an average of 50 ring down decays. The signal for $t < 0$ is shown to highlight the variations in the different measurements before the tracking circuit is triggered.

design of this apparatus allows us to non-perturbatively measure the VDF in any plasma source.

For comparison with the CW-CRDS measurements, LIF measurements of the argon Ion Velocity Distribution Function (IVDF) (Ref. 27) were also obtained for the same plasma conditions with the same diode laser and also with a dye laser. For the dye laser LIF measurements the, Ar II $3d'\ ^2G_{9/2}$ metastable state is optically pumped to the $4p'\ ^2F^0_{7/2}$ state by 611.6616 nm (vacuum wavelength) light from a CW Sirah Matisse-DR tunable ring dye laser employing rhodamine-6G dye. The dye laser is pumped with a 10 W Spectra-Physics Millennium Pro diode laser at 532 nm. The 1 W of output light from the laser is split, with 10% passing through an iodine cell and the other 90% mechanically chopped and transported to the plasma source laboratory through a 200 μm core, fused-silica, multimode fiber. The iodine cell emission is recorded with a photodiode for each scan of the dye laser wavelength. After passing through the iodine cell, the laser light is coupled into a Bristol Instruments 621-VIS wavemeter for real-time wavelength monitoring. Instead of injecting the laser light into the CRDS resonant cavity, the light is focused at the center of the discharge with a single lens at the top of the plasma source. The same injection optics are used for the diode laser LIF measurements. The LIF IVDF measurements are therefore along the direction of the magnetic field, whereas the CW-CRDS measurements are of the perpendicular velocity distribution function.

For the dye laser scheme, the fluorescent emission at 461.09 nm from the decay of $4p'\ ^2F^0_{7/2}$ state to the $4s'\ ^2D_{5/2}$ state is collected by another lens, collimated, and then coupled into an optical fiber. The intensity of the light emanating from the fiber some meters away is re-collimated, passed through a 1 nm wide filter centered at 461 nm, and measured with a visible light PMT. For the diode laser LIF scheme, 442.60 nm fluorescence radiation from the decay of the $4p^4D_{5/2}$ to the $4s^4P_{3/2}$ level is recorded with the same PMT and a filter centered on the 443 nm line. The intensity of the fluorescent emission from the excited state as a function of laser frequency is a direct measure of the IVDF in the region where the injected beam overlaps the collection volume. Note that the measurement volumes for the LIF and CRDS measurements were separated by 6 cm along the axis of the apparatus. Since the LIF PMT signal is composed of background spectral radiation, electron-impact-induced fluorescence radiation and electronic noise, a Stanford Research SR830 lock-in amplifier is used to eliminate signals not correlated with the laser modulation. Lock-in amplification is essential since electron-impact-induced emission is several orders of magnitude larger than the fluorescence signal.

VELOCITY DISTRIBUTION FUNCTION MEASUREMENTS

The CW-CRDS measured argon IVDF for a helicon plasma created with an rf power of 700 W, an antenna frequency of 13.56 MHz, a magnetic field strength of 1000 G in the source region, and a neutral gas pressure of 3 mTorr is shown in Fig. 5. The error bars shown in Fig. 5 are based on the maximum observed variation in the experimental values of the ring down times between multiple ring downs at a given wavelength because of the very small bore of the electromagnets used for the helicon source, the density drops very rapidly in the expansion region and the metastable density for the target CRDS state is quite low. The absorption coefficient for the $3d^4F_{7/2}$ state calculated from the measurements shown in Fig. 5 is $(5.1 \pm 0.2) \times 10^{-7}$ cm^{-1}. The absorption coefficient, $\propto(\nu)$, is related to the density of the initial state through

$$\propto(\nu) = \sigma_{ij}(\nu)N, \tag{6}$$

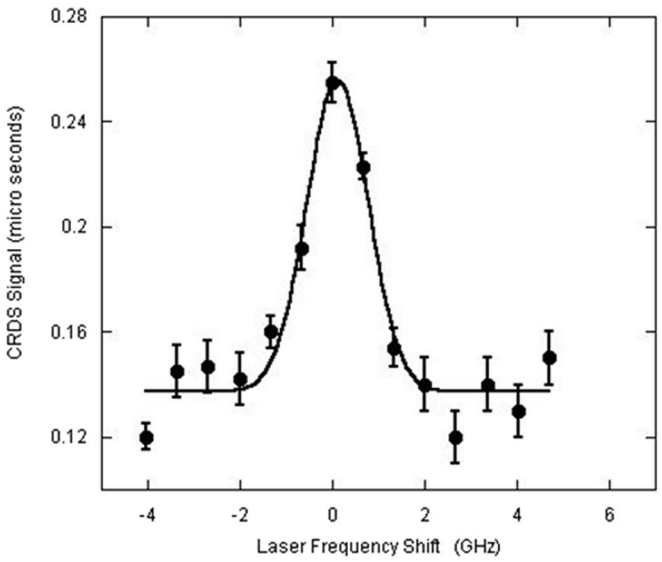

FIG. 5. CW-CRDS measurement of Ar II ion velocity distribution function using the diode laser (at 668.6138 nm) in CHEWIE. The DC offset arises from the ring down time in the absence of absorption by the plasma. The line averaged, perpendicular ion temperature obtained from the fit is 0.09 eV.

where N is the absolute density and $\sigma_{ij}(\nu)$ is the frequency dependent absorption cross section from state i to state j. For known values of the plasma temperature and the line shape broadening mechanisms, the absorption cross section is[28]

$$\sigma_{ij}(\nu) = \frac{g_i}{g_j}\frac{\lambda^4}{4\pi^2 c}\frac{A_{ji}}{\Delta\lambda_D}V(a,0)\sqrt{\pi\ln(2)}, \quad (7)$$

where g_i and g_j are the upper and lower state degeneracies, respectively, c is the speed of light, λ is the transition wavelength, A_{ji} is the spontaneous emission transition rate, $\Delta\lambda_D$ is the Gaussian component of the broadened absorption line shape due to Doppler broadening and $V(a, 0)$ is the Voigt function based on all the line width broadening mechanisms; where the parameter a is determined by the ratio of the Lorentzian and Gaussian components within the full line shape. For a predominantly Doppler broadened line shape, the value of $V(a, 0)$ is taken to be 1. For a general spectral line shape consisting of several broadening mechanisms, the values of a and $V(a, 0)$ can be calculated by applying standard Gaussian de-convolution techniques to the experimentally measured line.[28] For this purpose, commercially available software is used.

To determine the Doppler broadening needed for the absolute metastable density calculation using Eqs. (6) and (7), the IVDF is fit with a drifting Maxwellian distribution of the form

$$I_R(\nu) = I_R(\nu_o)e^{-m_i c^2(\nu-\nu_o)^2/2kT_i\nu_o^2}, \quad (8)$$

where ν_o is the rest frame frequency of the absorption line, m_i is the ion mass, and T_i is the ion temperature. The fit also provides a measure of the bulk ion flow speed. For a CW-CRDS measurement, these values are line-of-sight averages. Note that for magnetic field strengths less than 100 G (which is true of the magnetic field strength in the expansion chamber where the CW-CRDS measurement is performed), Zeeman splitting of the two circularly polarized, "sigma," absorption lines is ignorable.[29] A nonlinear fit of Eq. (8) to the CW-CRDS measured distribution yields a perpendicular ion temperature of 0.09 ± 0.03 eV and an average perpendicular flow of 70 ± 40 m/s. The errors are based on the uncertainties of the fit. The measured flow is consistent with a zero flow given that the accuracy of the laser wavelength measurement is equivalent to a 70 m/s uncertainty in the absolute flow speed determination.

For nearly the same plasma conditions, the parallel argon IVDF as measured with the diode laser and the dye laser LIF schemes are shown in Figs. 6 and 7 as a function of laser frequency relative to center of the laser scan range, respectively. A nonlinear fit of Eq. (8) to the diode LIF measured distribution yields a parallel ion temperature of 0.27 ± 0.03 eV and a bulk parallel flow 950 ± 100 m/s. For the dye laser data, the nonlinear fit of Eq. (8) to the measured distribution yields a parallel ion temperature of 0.21 ± 0.001 eV and a bulk parallel flow 1180 ± 100 m/s. Because the plasma density was so small in the expansion chamber, extremely long integration times (compared to the time scale of the scan of the laser frequency) were required to obtain measurable LIF signal levels with the diode laser. As we have shown in previous LIF experiments, such long integration times can lead to a significant overestimation of the ion temperature from the IVDF measurement; ~20%–30%.[30] Therefore, including the effects of excessive signal integration, the two parallel ion temperatures are consistent with each other.

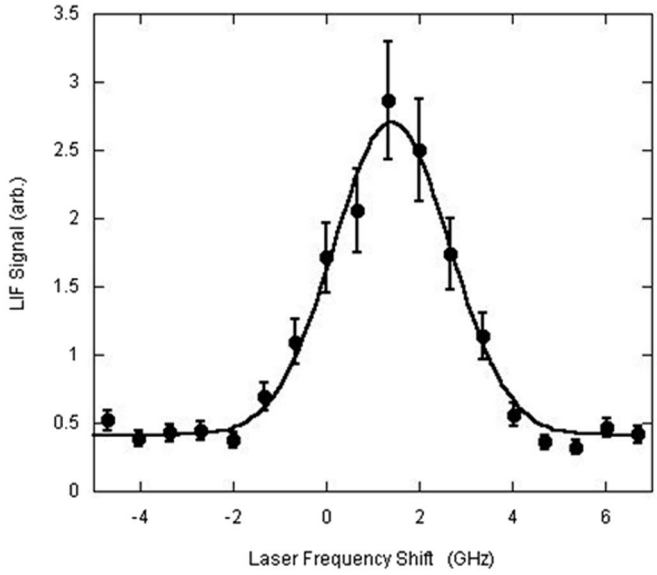

FIG. 6. LIF measurement of the parallel Ar II ion velocity distribution function on the plasma axis using the diode laser (at 668.6138 nm) in CHEWIE. The parallel ion temperature obtained from the fit is 0.27 ± 0.03 eV.

Since the CW-CRDS measurements are line-of-sight averaged, perpendicular ion temperature values, it is reasonable to consider the possible impact of a non-uniform radial perpendicular ion temperature profile on a line-of-sight averaged measurement. Assuming a parabolic perpendicular ion temperature profile (often observed in helicon sources[31]) with a peak temperature value T_{i0} at $r = 0$,

$$T_i(r) = T_{i0}[1 - (r/a)^2], \quad (9)$$

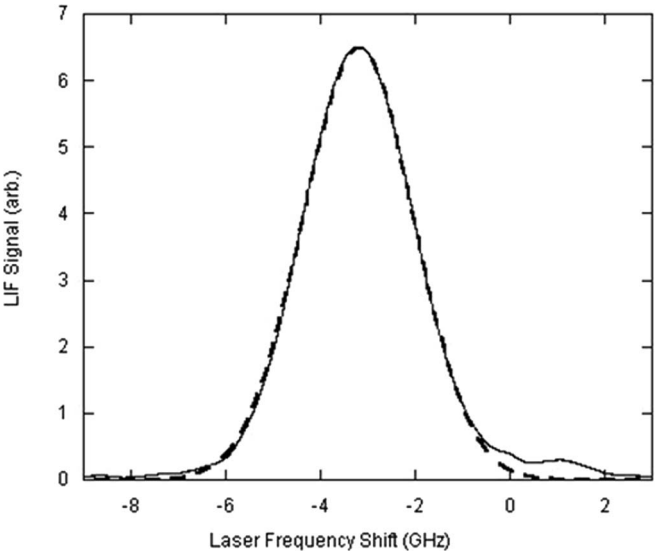

FIG. 7. LIF measurement of the parallel Ar II ion velocity distribution function on the plasma axis using the dye laser (at 611.6616 nm) in CHEWIE. The parallel ion temperature obtained from the fit (dashed line) is 0.21 $\pm$ 0.01 eV.

where $a = 5$ cm is the plasma radius, the averaged ion temperature is obtained from integrating over the temperature profile and normalizing by the $2a$ path length of the measurement. Equation (9) predicts that if the plasma were isotropic and had an on-axis ion temperature given by the parallel LIF measurements, a CRDS measurement would obtain a line-of-sight averaged perpendicular ion temperature of 0.13 eV.

Note also that the parallel LIF and the perpendicular CW-CRDS measurements were performed at different locations (due to a lack of experimental access for LIF). As shown in Fig. 1, the LIF measurements were performed through windows 6 cm closer to the source region than the line-of-sight averaged CW-CRDS measurements. Thus, the CW-CRDS location lies outside the strong magnetic field region near the source; the magnetic field strength at the CW-CRDS measurement position is half that of the value magnitude at the LIF measurement location. Previous LIF studies of ion temperatures in helicon sources have demonstrated a strong correlation between the magnetic field strength and ion temperature of a helicon plasma as well as larger parallel, compared to perpendicular, ion temperatures in helicon sources operating at pressures of only a few mTorr.[32] Given the effects of excessive lock-in integration, measurement location differences, and likely thermal anisotropy, the difference in ion temperatures obtained by the two methods is not a significant concern.

The argon ion absorption cross section at 668.6138 nm, calculated using Eq. (8) and data available from published tables,[33] is 8.5×10^{-13} cm^2. Integrating over the measured IVDF over all velocities (laser frequencies) to obtain the total absorption value and using an ion temperature of 0.09 eV, the calculated absolute, line-of-sight averaged density of the argon ion metastable state is $(1.2 \pm 0.03) \times 10^6$ cm^{-3}. Such a value for the metastable state density is consistent with collision-radiative models of the density of this metastable state in helicon sources at similar plasma parameters.[34]

In previous studies of expanding plasmas in a similar helicon source, several ion acceleration mechanisms have been identified that would explain the large parallel flow speeds observed in the parallel LIF IVDF measurements, e.g., formation of a double layer and/or magnetic moment conservation.[35] For the same conditions that led to large parallel flows in an expanding helicon plasma, two-dimensional LIF tomography studies demonstrated the absence of any significant perpendicular ion flows.[36] Thus, the very small flow, ~70 m/s, perpendicular ion flow obtained with the CW-CRDS technique is consistent with previous experimental results.

Additional studies designed to investigate the differences between IVDF measurements obtained through CW-CRDS and LIF are underway in a redesigned CHEWIE apparatus that has a more uniform axial magnetic field, improved optical access, and higher achievable rf powers. Now that the CW-CRDS technique has been demonstrated to work in argon plasma, the next step will be to replace the existing diode laser with diode lasers tuned to transitions in other species that have no viable LIF scheme, e.g., excited helium ion states. It is for such plasmas that the line-integrated CW-CRDS technique will provide the only means of performing IVDF measurements. For axially uniform, magnetized, cylindrical systems, CW-CRDS measurements performed along the axis of the system will provide radially resolved measurements of key quantities such as excited state density, parallel ion temperature, and parallel flow speed. All that is required is optical access for two ports along the cylindrical axis (but not necessarily at $r = 0$ cm).

In terms of the effectiveness of the CW-CRDS technique compared to LIF, we note that we were unable to obtain LIF measurements of the IVDF without resorting to a much more powerful LIF laser system. Thus, these experiments already demonstrate the advantage of CW-CRDS over LIF at plasma densities of 10^{10}–10^{11} cm^{-3} and target species temperatures of less than a few eV; parameters typical of plasma processing sources. Based on our expected performance improvements in the diagnostic, we expect to be able to push the measurement threshold down to 10^9–10^{10} cm^{-3} and the diagnostic should work up to the resolution of the ring down measurement system, approximately densities of 10^{13} cm^{-3}. We also note that the CW-CRDS technique, when coupled with a model of the state populations (such as a corona or collisional-radiative model) can provide absolute measurements of the ground state density of the target species; something that is only possible with an absolutely calibrated LIF system. Thus, this CW-CRDS technique has the potential to provide IVDF measurements over a much wider range of experimental conditions than LIF and for target species for which LIF is either impractical or simply impossible.

ACKNOWLEDGMENTS

We would like to thank Dr. Joseph Hodges from the National Institute of Standards and Technologies, Maryland, for his helpful suggestions regarding the CW-CRDS system. We also acknowledge fruitful discussions with Professor Chuji Wang from Mississippi State University and Dr. Cormac Corr from the Australia National University. This work was supported by NSF Award No. PHY-0902085.

[1] C. Charles, R. W. Boswell, and R. K. Porteus, J. Vac. Sci. Technol. A **10**, 398 (1992).
[2] C. Charles, J. Vac. Sci. Technol. A **11**, 157 (1993).
[3] C. Charles and R. W. Boswell, J. Vac. Sci. Technol. A **13**, 2067 (1995).
[4] F. F. Chen, X. Jiang, and J. D. Evans, J. Vac. Sci. Technol. A **18**, 2108 (2000).
[5] A. J. Perry and R. W. Boswell, Appl. Phys. Lett. **84**, 332 (2004).
[6] S. G. Ingram and N. S. J. Braithwaite, J. Phys. D **21**, 1496 (1988).
[7] Z. Harvey, S. Chakraborty Thakur, A. Hansen, R. A. Hardin, W. S. Przybysz, and E. E. Scime, Rev. Sci. Instrum. **79**, 10F314 (2008).
[8] I. A. Biloiu and E. Scime, Phys. Plasmas **17**, 113508 (2010).
[9] T. E. Sheridan and J. Goree, Phys. Rev. E **50**, 2991 (1994).
[10] R. W. Boswell, Plasma Phys. Controlled Fusion **26**, 1147 (1970).
[11] A. B. Altukhov, E. Z. Gusakov, M. A. Irzak, M. Krämer, B. Lorenz, and V. L. Selenin, Phys. Plasmas **12**, 022310 (2005).
[12] Jong-Gu Kwak, S. J. Wang, S. K. Kim, and Suwon Cho, Phys. Plasmas **13**, 074503 (2006).
[13] A. M. Keesee, R. Boivin, and E. E. Scime, Rev. Sci. Instrum. **75**, 4091 (2004).
[14] A. Aanesland, L. Liard, G. Leray, J. Jolly, and P. Chabert, Appl. Phys. Lett. **91**, 1 (2007).
[15] G. Severn, L. Dongsoo, and N. Hershkowitz, Rev. Sci. Instrum. **78**, 116105 (2007).
[16] A. O'Keefe and D. A. G. Deacon, Rev. Sci. Instrum. **59**, 2544 (1988).
[17] K. W. Busch and M. A. Busch, *American Chemical Society Symposium Series*, Vol. 720 (ACS Publications, Washington DC, USA, 1999).
[18] G. Berden, R. Peeters, and G. Meijer, Int. Rev. Phys. Chem. **19**, 565 (2000).

[19]B. Paldus and A. Kachanov, Can. J. Phys. **83**, 975 (2005).
[20]M. Mazurenka, A. J. Orr-Ewing, R. Peverall, and G. A. D. Ritchie, Annu. Rep. Prog. Chem., Sect. C: Phys. Chem. **101**, 100 (2005).
[21]G. Berden and R. Engeln, *Cavity Ring-Down Spectroscopy: Techniques and Application* (Wiley, Chichester, UK, 2009).
[22]C. Wang, J. Anal. At. Spectrom. **22**, 1347 (2007).
[23]D. Romanini, A. A. Kachanov, N. Sadeghi, and R. Stoeckel, Chem. Phys. Lett. **264**, 316 (1997).
[24]L. Tao, A. P. Yalin, and N. Yamamoto, Rev. Sci. Instrum. **79**, 115107 (2008).
[25]I. D. Sudit and F. F. Chen, Plasma Sources Sci. Technol. **3**, 162 (1994).
[26]S. Chakraborty Thakur, "Understanding plasmas through ion velocity distribution function measurements," Ph.D. dissertation (West Virginia University, 2010).
[27]E. Scime, P. A. Keiter, M. W. Zintl, M. M. Balkey, J. L. Kline, and M. E. Koepke, Plasma Sources Sci. Technol. **7**, 186 (1998).
[28]C. Wang, F. J. Mazzotti, G. P. Miller, and C. B. Winstead, Appl. Spectrosc. **56**, 386 (2002).
[29]R. F. Boivin, West Virginia University Plasma Physics Lab Report PL-050; see supplemental material in S. A. Cohen, N. S. Siefert, S. Strange, R. F. Boivin, E. E. Scime, and F. M. Levinton, Phys. Plasmas **10**, 2593 (2003).
[30]E. E. Scime, R. Hardin, A. M. Keesee, C. Biloiu, and X. Sun, Phys. Plasmas **14**, 043505 (2007).
[31]J. L. Kline, E. Scime, R. Boivin, A. M. Keesee, and X. Sun, Plasma Sources Sci. Technol. **11**, 413 (2002).
[32]J. L. Kline, E. Scime, R. Boivin, A. M. Keesee, X. Sun, and V. Mikhailenko, Phys. Rev. Lett. **88**, 1950 (2002).
[33]Yu. Ralchenko, A. E. Kramida, J. Reader, and NIST ASD Team, *NIST Atomic Spectra Database* (version 4.0) (2010); see http://physics.nist.gov/asd.
[34]A. M. Keesee and E. E. Scime, Plasma Sources Sci. Technol. **16**, 742 (2007).
[35]I. A. Biloiu and E. Scime, Phys. Plasmas **17**, 113508 (2010); **17**, 113509 (2010).
[36]I. Biloiu, E. Scime, and C. Biloiu, Plasma Sources Sci. Technol. **18**, 025012 (2009).